Velocity analysis using both reflections and refractions in seismic interferometry

GEOPHYSICS. VOL. 76, NO. 5 (SEPTEMBER-OCTOBER 2011); P. SA83–SA96, 20 FIGS.
10.1190/GEO2011-0008.1

Velocity analysis using both reflections and refractions in seismic interferometry

Simon King[1] and Andrew Curtis[1]

ABSTRACT

The Green's function between two receiver locations can be estimated by crosscorrelating and summing the recorded Green's functions from sources on a boundary that surrounds the receiver pair. We demonstrate that when two receivers are positioned far from the source boundary in a marine-type acquisition geometry, the crosscorrelations (the Green's functions before summation over the source boundary) are dominated by reflected energy which can be used in a semblance analysis to determine the seismic velocity and thickness of the first layer. When these crosscorrelations are summed over the boundary of sources, the resulting Green's function estimates along a receiver array contain nonphysical or spurious refracted energy. We illustrate that by using a further semblance analysis, the most prominent nonphysical refracted energy occurs prior to the direct arrival and determines the remaining refraction velocities of deeper layers (or interval velocities in the case of a subsurface with homogeneous layers). We demonstrate the velocity analysis procedure on a single layer over half-space model, a three layer over a half-space model, and a more realistic model based on a North Sea oil field.

INTRODUCTION

A seismic image represents subsurface interfaces or points at which the (an)elastic properties of the earth vary significantly in magnitude over a spatial length scale that is short relative to the wavelength of seismic waves. Before an image can be computed, we require an accurate estimation of the elastic property variations over length scales of a wavelength or longer, often referred to as a seismic velocity model. Usually geophysicists estimate the subsurface seismic velocities by analyzing the kinematic properties of recorded traveltimes as a function of the source-receiver offset.

In this paper, we study the moveout properties of reflected and refracted Green's function estimates that have been redatumed to a receiver array located beneath the free surface by using seismic interferometry. We aim to estimate the seismic velocity using these moveout properties. In seismic interferometry, the Green's function $G(\mathbf{x}_B, \mathbf{x}_A, \omega)$, that would be recorded if a transient source was fired at a receiver location $\mathbf{x}_A$ (often termed the "virtual source" location) and recorded at an arbitrary receiver positioned at $\mathbf{x}_B$, can be extracted by crosscorrelating and summing the Green's functions recorded at $\mathbf{x}_A$ and $\mathbf{x}_B$ due to an illuminating boundary of monopolar and dipolar sources (Wapenaar, 2004; van Manen et al., 2005, 2006; Wapenaar and Fokkema, 2006). In practice, it is difficult to realize a source boundary with both of the source types, but Wapenaar and Fokkema (2006) show that if sources lie in the far-field, the homogeneous Green's function $G(\mathbf{x}_B, \mathbf{x}_A, \omega) + G^*(\mathbf{x}_B, \mathbf{x}_A, \omega)$ (i.e., the Green's function plus its time reverse) can be approximated using only monopolar sources:

$$G(\mathbf{x}_B, \mathbf{x}_A, \omega) + G^*(\mathbf{x}_B, \mathbf{x}_A, \omega) \approx \frac{2}{\rho c} \oint_{\partial S} G(\mathbf{x}_B, \mathbf{x}, \omega) G^*(\mathbf{x}_A, \mathbf{x}, \omega) d^2\mathbf{x}, \quad (1)$$

where ω is the angular frequency, ρ and c are the density and velocity which are assumed to be constant at position $\mathbf{x}$, $G(\mathbf{x}_i, \mathbf{x}, \omega)$ represents the frequency-domain Green's function between a monopolar source at $\mathbf{x}$ on the boundary ∂S and a receiver positioned at $\mathbf{x}_i$, and the asterisk denotes complex conjugation. By reciprocity, Curtis et al. (2009) show that the Green's function between two sources can also be estimated given their recordings on a boundary of receivers. Furthermore, if we have two boundaries, one of sources and one of receivers, Curtis and Halliday (2010b) show that the Green's function between an isolated source and receiver can be extracted using the appropriate crosscorrelation and/or cross-convolution operations. Here, we focus on seismic interferometry

Manuscript received by the Editor 12 January 2011; revised manuscript received 31 March 2011; published online 7 November 2011.
[1]The University of Edinburgh, School of GeoSciences, and Edinburgh Collaborative of Subsurface Science and Engineering (ECOSSE), Edinburgh, UK. E-mail: s.j.king@sms.ed.ac.uk; andrew.curtis@ed.ac.uk.

between two receivers and adopt an acquisition geometry similar to those employed in marine seismic settings, but our results are also pertinent to other forms of interferometry.

To estimate the Green's function with the correct kinematic and amplitude properties, theory dictates that the source boundary must enclose the receiver pair (indicated by the closed integral in equation 1). In exploration seismology, it is usual for the source boundary to be partially complete resulting in an erroneous Green's function contaminated with artifacts known as nonphysical arrivals (Snieder et al., 2006). In this paper, we use the moveout of such artifacts to obtain model subsurface information.

The retrieval of reflections and refractions in seismic interferometry has received both theoretical and applied attention. Bakulin and Calvert (2006) and Mehta et al. (2007) showed that by crosscorrelating recordings in a horizontal well at depth, reflections that are relatively free from the distortive effects of a complex overburden can be synthesized. Theoretically, Snieder et al. (2006) extract the primary reflection by crosscorrelating the direct arrival with the primary reflection. Tatanova et al. (2008) present a similar derivation but focus on the contributions obtained when crosscorrelating refracted energy.

Little attention has been focused on the possibilities of using seismic interferometry to recover information about the long-wavelength seismic velocity model in exploration seismology. Examples that do exist estimate the seismic velocity using interferometric refractions (Mikesell et al., 2009) and reflections (King et al. 2011), respectively. The former authors show that the crosscorrelation of refracted energy leads to a spurious linear refraction that passes through the origin and whose gradient is equal to the slowness of the refracting layer. The latter authors demonstrate that interfering primary and multiple energy in the so-called correlation gather (defined in the next section) can be used to find the root mean square (rms) and interval velocities of a multilayered model.

We study the retrieval of reflected and refracted Green's functions in a marine seismic setting. We adopt and combine the approaches of King et al. (2011) and Mikesell et al. (2009) to investigate the seismic velocity of subsurface strata. We perform a semblance analysis on the crosscorrelated wavefield between two receivers to estimate the velocity and layer thickness of the first layer (King et al., 2011). We then show that when the receiver array is positioned at far offset from the illuminating source array, the estimated Green's functions are dominated by nonphysical refracted energy prior to the direct arrival, similar to that identified by Mikesell et al. (2009), that can be used to characterize the seismic velocity of deeper layers using a semblance analysis. We demonstrate our velocity analysis procedure on a single layer over half-space and a three layer over half-space acoustic models. Finally, we demonstrate this procedure on a more realistic 2.5D model based on a North Sea oil field.

SEISMIC INTERFEROMETRY IN EXPLORATION SEISMOLOGY

Single layer over a half-space model

Figure 1 shows a single layer over half-space homogeneous model and acquisition geometry. The model comprises an upper layer with a velocity of 1500 m/s separated from a half-space with velocity of 2500 m/s by a planar interface at 150 m depth. A boundary of 100 sources, at 5 m depth, illuminates 501 receivers, at 15 m depth. Receiver r_0 is positioned directly beneath source 85. The remaining 500 receivers form an array. In this example, we produce synthetic data by firing each source on the boundary ∂S in turn and modeling the full wavefield Green's functions to all receivers by using a 2D acoustic finite-difference code (Robertsson et al., 1994).

The time-domain integrand of equation 1 (i.e., the set of crosscorrelations between a fixed receiver pair before summation over the boundary of sources) can be displayed as a group of traces commonly referred to as the correlation gather (Mehta et al., 2008). Figure 2a shows the correlation gather for receivers r_0 and r_1. The distance between r_0 and r_1 is 560 m. The crosscorrelation operation subtracts the phase of the wavefield recorded at r_0 from the phase of the wavefield recorded at r_1. Hence, wavefields in the correlation gather occur at the traveltime differences between waves recorded at the two receivers. Reflected wave energy in the correlation gather arrive at traveltimes $\delta\mathbf{t}$ according to the following equation:

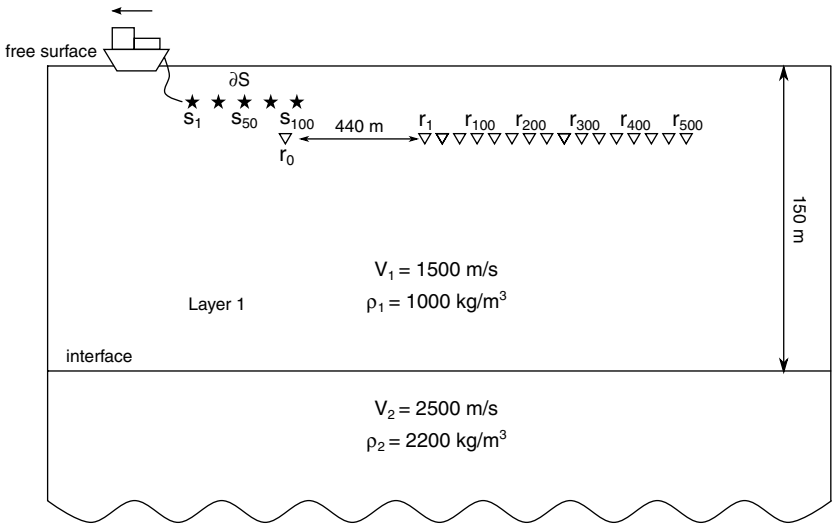

Figure 1. Single layer over half-space model showing the acquisition geometry. Velocities (V_1 and V_2) and densities (ρ_1 and ρ_2) are shown. Sources and receivers are denoted by stars and triangles, respectively. The source boundary ∂S containing 100 sources at 5-m depth illuminates 501 receivers at 15-m depth. Sources are spaced every 8 m. An isolated receiver r_0 is positioned directly beneath source 85. The remaining 500 receivers form an array, 440 m from source 100, and are separated at 4-m intervals.

$$\delta \mathbf{t} = \frac{\sqrt{x_{r_j}^2 + (2b_{r_j}Z_1 \pm z_s \pm z_{r_j})^2}}{V_1} - \frac{\sqrt{x_{r_i}^2 + (2b_{r_i}Z_1 \pm z_s \pm z_{r_i})^2}}{V_1}, \quad (2)$$

where x_{r_j} and x_{r_i} are the horizontal offsets between the active source and farthest jth and nearest ith receiver, respectively, $b_{r_j}(b_{r_i})$ is the number of bounce points from the bottom interface located at depth Z_1 that occur between the source and receiver position, z_s is the depth of the source, $z_{r_j}(z_{r_i})$ is the depth of each receiver, and V_1 is the seismic velocity of the top layer of the medium. The sign of z_s is negative when waves are downgoing from the source, and positive when waves are upgoing, and the sign of $z_{r_j}(z_{r_i})$ is negative when waves are upgoing at the receiver and positive when waves are downgoing.

In the following traveltime interpretation, we assume that V_1 and Z_1 are known and that waves are downgoing at the source and upgoing at the receiver. Figure 2b displays a reflective traveltime interpretation of the correlation gather using equation 2. For clarity, we do not interpret every arrival but a significant number to provide the reader with a good impression of the correlation gather properties. The V-shaped traveltime curves represent the crosscorrelation of increasing orders of reflections, primary (P) or multiple (MN) at r_1, where N is the multiple order (e.g., $b_{r_j} > 0$ in equation 2), with the direct arrival D ($b_{r_i} = 0$) at r_0. The smooth traveltime curves represent the crosscorrelations between reflections at both receivers (see the left-hand side of Figure 2b and caption for further definitions). Figure 2c shows the Green's function estimate after summing the correlation gather over all source numbers. Stationary energy in the correlation gather (i.e., extrema in Figure 2a and b — energy that varies slowly with respect to the boundary source location) will add constructively and provides the dominant contribution to the Green's function estimate in Figure 2c (Snieder, 2004; van Manen et al., 2005, 2006). Active sources that produce stationary energy are called stationary-phase sources. Apart from the incoherent noise obtained prior to the primary reflection P, the estimated Green's function shows reasonable agreement with the true Green's function in Figure 2d.

In exploration seismology, most receivers are positioned at far offset from the available sources. Hence, consideration of the equivalent panels for example receivers r_{200} and r_{400} would provide a more likely or practical scenario than having a receiver at r_0 as shown above. Figure 3a shows the correlation gather for receivers r_{200} and r_{400} with traveltime interpretation (using equation 2). The distance between r_{200} and r_{400} is 800 m. Instead of distinct extrema, as displayed in Figure 3a, near-horizontal arrivals which represent the crosscorrelation between reflections provide the stationary energy to the Green's function estimate (Figure 3b). These linear arrivals should not be confused with those generated by the crosscorrelation of refractions, for example the "virtual refraction," as observed in Mikesell et al. (2009). In fact, although both receivers are positioned past the critical offset (= 210 m) for all 100 sources, refractions are not observable in the correlation gather because their amplitudes are masked by those of reflections. Refraction amplitudes decrease rapidly with increasing range as $1/(L^{3/2}x_{r_{i,j}}^{1/2})$, where $L = x_{r_{i,j}} - x_c$ and x_c is the critical offset (Kennett, 1977). Reflections dominate the correlation gather because their amplitudes decrease only as $1/x_{r_{i,j}}$.

Positive arrival times in the estimated Green's function in Figure 3b show reasonable agreement to those in the positive-time true Green's function in Figure 3c. The reflected energy before 0.5 s in the correlation gather interferes destructively, resulting in an estimated Green's function at negative times, which shows little agreement to the true homogeneous Green's function. Despite this, it is clear from Figure 3d, which shows an enlarged portion of the Green's function within the box in Figure 3b, that we obtain coherent arrivals of crosscorrelated energy separated at constant

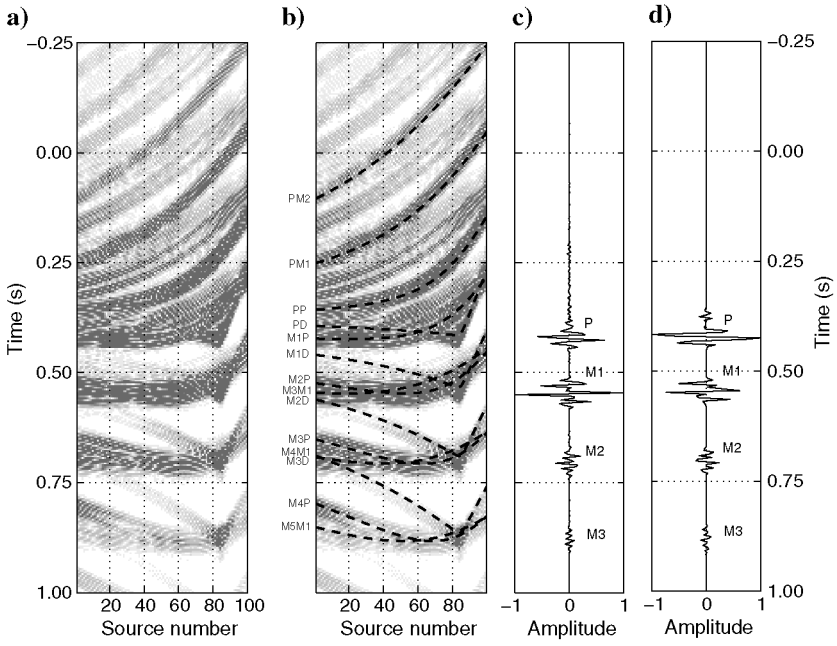

Figure 2. (a) Correlation gather for r_0 and r_1, with (b) reflective traveltime interpretation for single layer over half-space model. (c) Normalized Green's function after summation over source number in (a). (d) Normalized true Green's function. In (b), we annotate reflected crosscorrelational energy (dashed black curves) and assume the convention "M1P" for example, which refers to the crosscorrelation of the first-order multiple (M1) at r_1 with the primary reflection (P) at r_0. Abbreviations are D — direct arrival, P — primary reflection, M1 — first-order multiple, M2 — second-order multiple, and so on. In (c) and (d), we include an interpretation of arrivals.

−0.16 s intervals. These arrivals result from the summation of the crosscorrelational energy between pairs of refracted waves according to the following traveltime equation:

$$\delta \mathbf{t} = \left(\frac{x_{r_j}}{V_2} + \frac{(2b_{r_j}Z_1 \pm z_s \pm z_{r_j}) \cos\,\theta_c}{V_1} \right) - \left(\frac{x_{r_i}}{V_2} + \frac{(2b_{r_i}Z_1 \pm z_s \pm z_{r_i}) \cos\,\theta_c}{V_1} \right), \quad (3)$$

where θ_c is the critical angle at the interface as determined by Snell's law. When $b_{r_j}(b_{r_i}) \geq 2$, the wavefield represents a surface-related refraction multiple (Meissner, 1965). For example, Figure 4 shows a sketch of a second-order refraction multiple. In Figure 3d, the energy at −0.16 s represents the third-order refraction multiple R3 ($b_{r_i} = 4$) at r_{200} crosscorrelated with the singly refracted arrival R ($b_{r_j} = 1$) at r_{400}. Similarly, the energy at approximately −0.32 s, −0.48 s, −0.64 s, and −0.80 s represent increasing orders of refraction multiples RN, where $N \geq 4$ at r_{200} crosscorrelated with the singly refracted arrival R at r_{400}. Tatanova et al. (2008) term the crosscorrelation of refracted energy that appears prior to the actual refracted arrival as satellite waves. This refracted energy is not observable in the raw correlation gather but is clearly visible in the Green's function estimate after the reflected energy at negative times has canceled through destructive interference.

These nonphysical refractions are more obvious when we produce the estimated Green's function along the receiver array. Figure 5 shows the virtual source gather obtained by crosscorrelating the records at r_{200} with receivers $r_1 - r_{500}$ using equation 1. The estimated Green's functions for $r_1 - r_{199}$ have been time reversed so that the moveout properties resemble those of a usual source gather. We apply this operation to traces left of the virtual source in all virtual source gathers that follow. The Green's function estimates are dominated by linear and largely nonphysical refracted arrivals (see dashed lines in Figure 5 for their traveltime interpretation). The arrival marked RR is the "virtual refraction," as described by Mikesell et al. (2009). The circles mark the coherent arrivals displayed in Figure 3d. We observe high-amplitude reflection events that asymptote to the nonphysical refractions R2R, R3R, R4R, and R5R, respectively. For example, the second-order reflection multiple is an asymptote to R3R. However, we do not observe the characteristic reflection hyperbola for two reasons. First, we require sources positioned at distinct reflected wave stationary-phase locations and in their associated Fresnel zones. Several stationary-phase sources (particularly those that lie close to and above the virtual source receiver as in Figure 2a for example) are not available in typical marine seismic surveys like this one. Second, the crosscorrelation of reflected waves excited by sources near the surface produce a reflected Green's function whose amplitude is smaller than that of the true reflected wave because obtaining the true amplitude requires sources at depth (Forghani and Snieder, 2010). On the other hand, refracted energy from sources that are past the critical offset (= 210 m) at the virtual source receiver will add constructively in the estimated Green's function. Therefore, the stationary-phase requirement for nonphysical refracted waves is less restrictive than for reflected waves, and hence, for the model shown here the crosscorrelation of r_{200} with $r_1 - r_{500}$ will produce a Green's function dominated by refraction-associated events.

VELOCITY DETERMINATION USING REFLECTIONS AND NONPHYSICAL REFRACTIONS

Although we do not observe reflection hyperbola in Figure 5, the reflected energy in the correlation gather (Figure 3a) is still useful for determining the unknown velocity V_1 and layer thickness Z_1 of the first layer (King et al., 2011). By choosing different estimates of V_1 and Z_1 and different values of $b_{r_j}(b_{r_i})$ in equation 2, we compute the traveltime difference moveout curves and measure the associated signal coherency in the correlation gather. Here, we use semblance as the coherence measure which is defined as

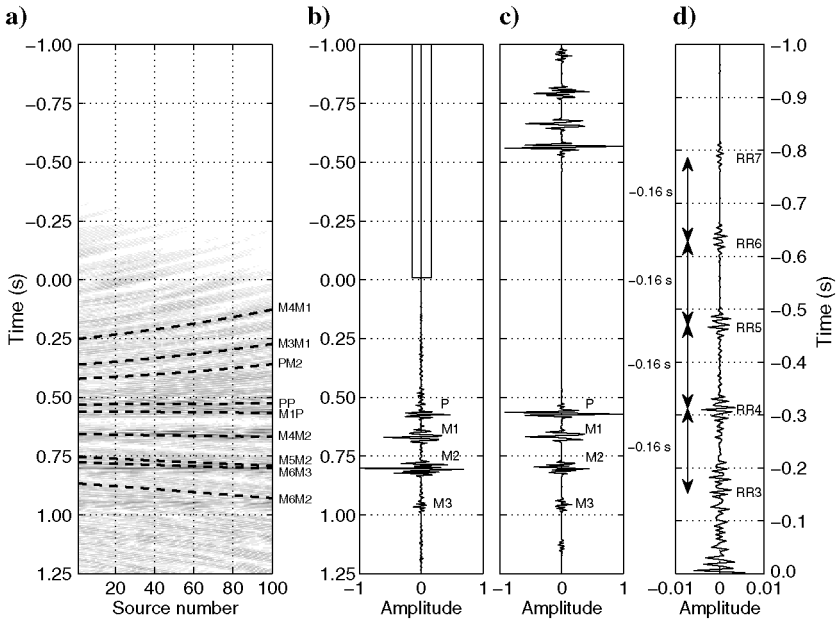

Figure 3. (a) Correlation gather for r_{200} and r_{400} with reflective traveltime interpretation for single layer over half-space model. (b) Normalized Green's function after summation over source number in (a). (c) Normalized true Green's function. (d) Enlargement showing the Green's function in the box in (b). In (a), the annotation convention follows that of Figure 2.

$$S_c = \frac{1}{(b_{r_i} \times b_{r_j})} \sum_{i=1}^{b_{r_i}} \sum_{j=1}^{b_{r_j}} \frac{E_{i,j}^{\text{out}}}{N \cdot E_{i,j}^{\text{in}}} \qquad 0 \le S_c \le 1, \quad (4)$$

where N is the number of sources or "traces" in the correlation gather and the output energy E_{out} and input energy E_{in} are defined as

$$E_{i,j}^{\text{out}} = \sum_{t(k)=\delta t - t/2}^{\delta t + t/2} \left\{ \sum_{\ell=1}^{N} f_{i,j,\ell,t(k)} \right\}^2 \quad (5)$$

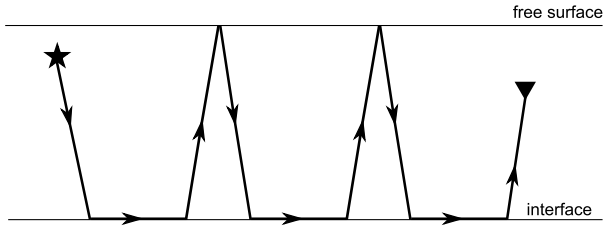

Figure 4. Sketch showing a second-order refraction multiple.

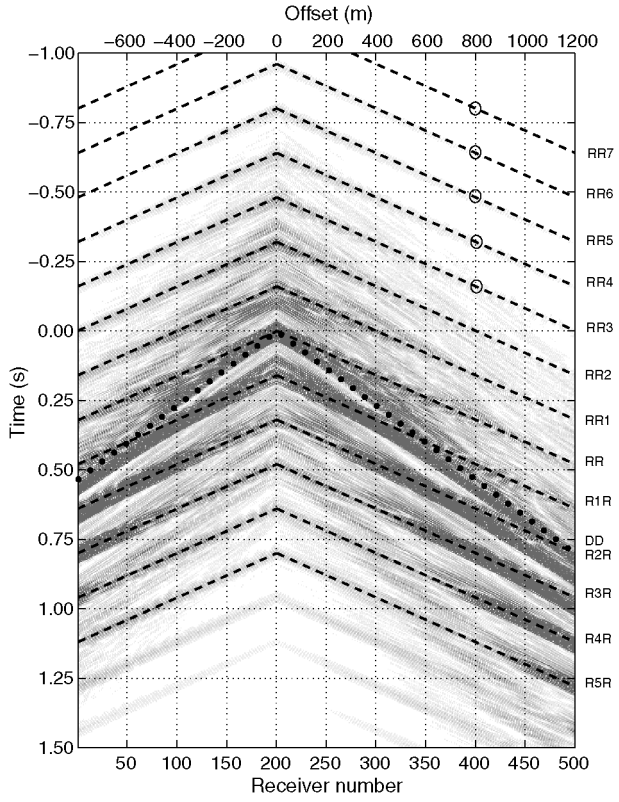

Figure 5. Virtual source gather for single layer over half-space model. The virtual source is positioned at r_{200}. On the right-hand side, the direct and nonphysical refracted Green's functions are annotated using the convention outlined in the caption to Figure 2. Abbreviations are D — direct arrival, R — singly refracted arrival, R1 — first-order refraction multiple, R2 — second-order refraction multiple and so on. Circles represent the traveltime of the coherent arrivals in Figure 3d. Traces at negative offsets have been reversed in time to emulate a more familiar form of the (virtual) source gather.

and

$$E_{i,j}^{\text{in}} = \sum_{t(k)=\delta t - t/2}^{\delta t + t/2} \sum_{\ell=1}^{N} f_{i,j,\ell,t(k)}^2, \quad (6)$$

where f is a function of V_1, Z_1, b_{r_i}, b_{r_j} and is the amplitude value at the ℓth source at time δt within a time window $[-t/2 t/2]$. After summing over b_{r_i} and b_{r_j} in equation 4, we create a velocity-layer-thickness spectrum. In all examples, we use a time-window length equal to 20 ms. Figure 6a shows the velocity-layer-thickness spectrum computed using all 100 sources and energy up to the

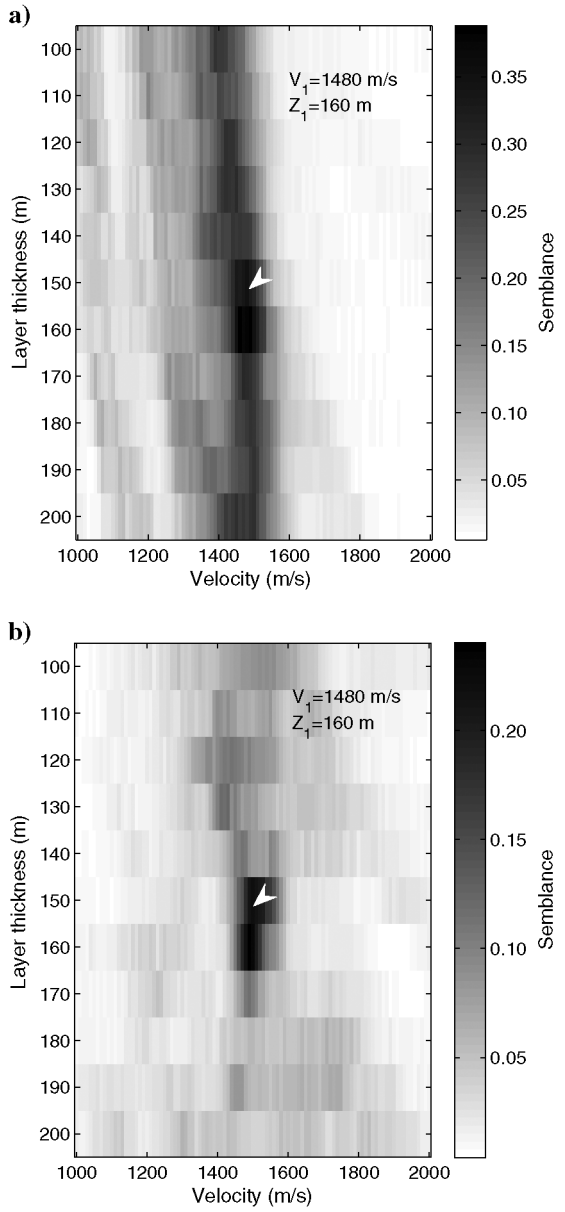

Figure 6. (a) Velocity (V_1) — layer thickness (Z_1) spectrum computed from the correlation gather in Figure 3a using energy up to the third-order multiples. (b) As for (a) but for the correlation gather in Figure 2a. The V_1 and Z_1 values noted in the top right-hand corners correspond to the peak of maximum semblance. The arrowheads denote the actual parameters of velocity and layer thickness.

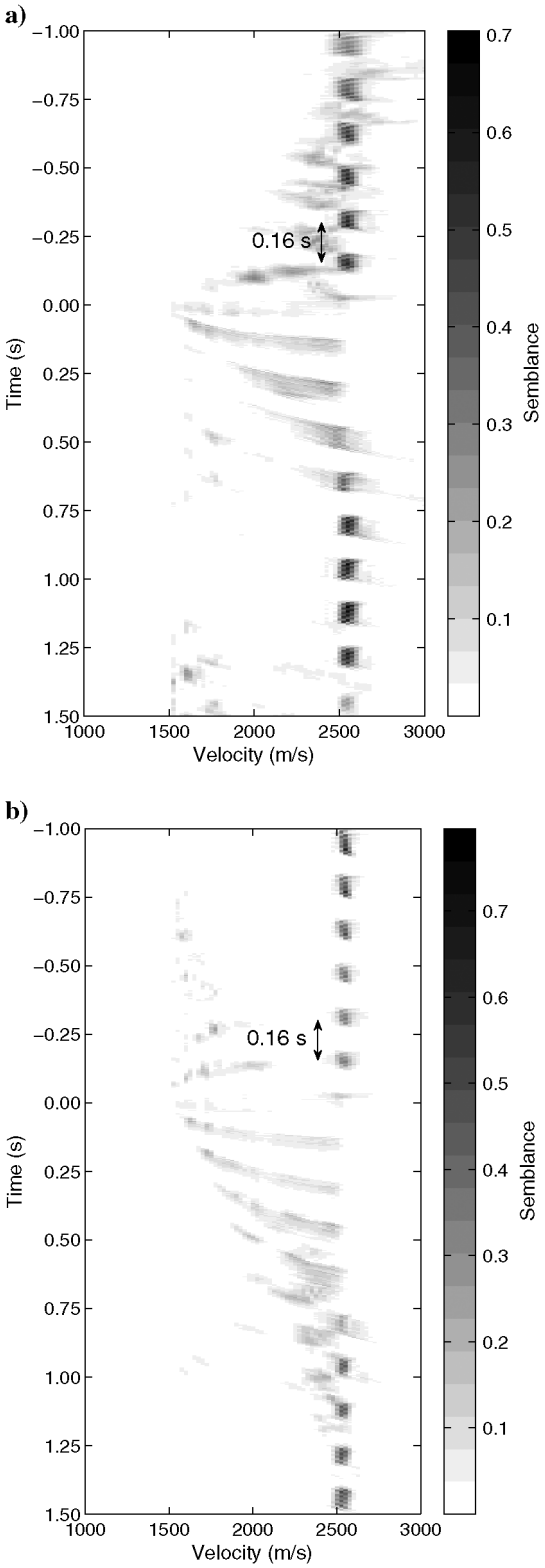

Figure 7. Velocity (V_2) — time (τ) spectrum computed using (a) receivers $r_1 - r_{200}$ and (b) receivers $r_{200} - r_{500}$ from the virtual source gather in Figure 5.

third-order multiples ($b_{r_{i,j}} = 4$) from the correlation gather in Figure 3a. We see a peak centered at $V_1 = 1480$ m/s and $Z_1 = 160$ m, close to the correct parameters of velocity and layer thickness; however, the estimate is smeared toward higher and lower thicknesses. Figure 6b shows the corresponding velocity-layer-thickness spectrum from the correlation gather in Figure 2a. In comparison, we achieve a better-constrained peak. The reason for this difference can be explained by observing the two respective correlation gathers. The correlation gather in Figure 2a shows reflected energy which is well-defined in space and time. This leads to a good estimate of V_1 and Z_1 in Figure 6b. The separation of reflected energy is less clear in the correlation gather of Figure 3a and the estimate of V_1 and Z_1 in Figure 6a is more smeared as a result. Nevertheless, we demonstrate that the reflected energy in the correlation gathers contains useful model information.

In addition, the linear nonphysical refracted energy in the virtual source gather (Figure 5) contains information about the velocity of the half space. We create a second velocity spectrum by stacking energy with the linear traveltime equation

$$t = \tau + \frac{x}{V}, \tag{7}$$

where τ is the traveltime at the virtual source position and x is the offset from the virtual source to a receiver. Equation 7 is equivalent to the slant-stack equation $t = \tau + px$, where p is the ray parameter (Yilmaz, 2001). Hence, the resultant velocity spectrum is a "pseudo" slant-stack gather. In the slant-stack domain, we would expect reflections to map as ellipses and refractions to map as isolated points of energy (Diebold and Stoffa, 1981). However, as we do not observe a reflection hyperbola in Figure 5, we expect to see isolated peaks that correspond to the correct velocity V_2 of the half space.

We now adopt the more usual form of semblance (i.e., the fraction and summations involving b_{r_i} and b_{r_j} are removed in equation 4, and N becomes the number of traces in the virtual source gather). Figure 7a shows the $\tau - V_2$ spectrum obtained by using equation 7 for receivers $r_1 - r_{200}$. Note that this spectrum that uses traces to the left of the virtual source position and all others that follow was created by using the traces in the virtual source gather (i.e., after the traces were reversed in time). Figure 7b shows the corresponding $\tau - V_2$ spectrum for receivers $r_{200} - r_{500}$. In both spectra, we observe a set of peaks at positive times at the correct velocity of 2500 m/s. Between 0 s and 0.5 s, we observe elliptical energy corresponding to the reflections. Peaks corresponding to refracted energy between 0 s and 0.5 s, and specifically the peak corresponding to the virtual refraction RR (Mikesell et al., 2009) at $\tau = 0$ s, are smeared because of the interference of reflected energy in the virtual source gather. At negative times, we observe little reflected energy in either spectra but again see a further set of distinct peaks that have the correct velocity of 2500 m/s. Note, although the peaks at negative times have the same traveltime as the arrivals in Figure 3d, the traveltime τ here is the traveltime at the virtual source position and not at the receiver. We obtain sharper peaks in Figure 7b because we use 100 more receivers in equation 7 than in Figure 7a.

We can also use the traveltime difference between peaks $\Delta\tau$ to compute the thickness Z_1 of the refracting layer by using the equation

$$Z_1 = \frac{\Delta\tau V_1 V_2}{2\sqrt{V_2^2 - V_1^2}}. \quad (8)$$

Assuming we know $V_1 = 1480$ m/s from Figure 6, and taking $V_2 = 2500$ m/s and $\Delta\tau = 0.16$ s as the time between peaks in Figure 7, the layer thickness by using equation 8 is equal to 147 m. This agrees well with the alternative estimate made using the correlation gather (Figure 6).

Three layer over a half-space model

We adopt the same approach as above to determine the interval velocities for a three layer over a half-space homogeneous acoustic model (Figure 8). Figure 9a shows the correlation gather for receivers r_{200} and r_{400}, respectively. An interpretation of arrivals, such as that displayed in Figures 2b and 3a, is more difficult due to the overlapping wavefields created by the addition of two extra interfaces. Figure 9b displays the interferometric Green's function estimate; note the predominant reflected and refracted energy arrives at

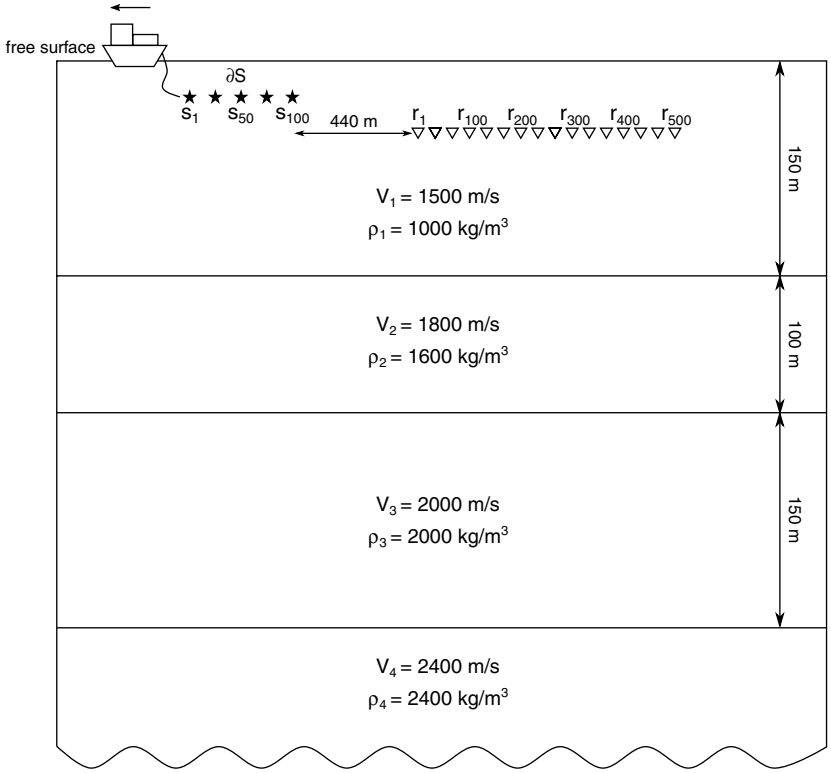

Figure 8. Three layer over a half-space model showing velocities (V_1, V_2, V_3, and V_4) and densities (ρ_1, ρ_2, ρ_3, and ρ_4). Acquisition geometry same as in Figure 1 but without receiver r_0.

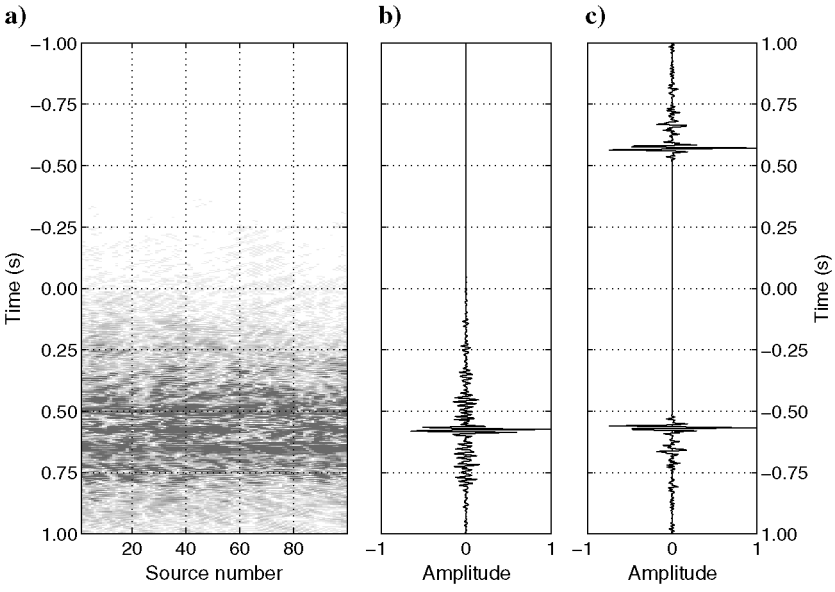

Figure 9. (a) Correlation gather for r_{200} and r_{400} for three layer over a half-space model. (b) Normalized Green's function after summation over source number in (a). (c) Normalized true Green's function.

positive times. Figure 9c shows the true Green's function for comparison. Figure 10 displays virtual source gathers with the virtual source positioned at r_{200} and r_{250}, respectively.

The correlation gather is dominated by reflected energy, although the virtual source gather also includes nonphysical refracted energy. As above, we exploit these differences to produce an estimate of the seismic velocity. Figure 11 displays the velocity-layer-thickness spectrum computed by using all 100 sources and energy up to third-order multiples from the correlation gather in Figure 9a. We obtain a well-constrained peak close to the correct first-layer velocity and layer-thickness parameters, but also observe a more prominent ridge toward higher and lower thicknesses for the reasons previously described.

Figure 12a shows the $\tau - V$ spectrum obtained by using equation 7 for $r_1 - r_{200}$ in the virtual source gather of Figure 10a. Figure 12b shows the corresponding $\tau - V$ spectrum for $r_{200} - r_{500}$. At positive times in both spectra, we observe elliptical energy and spurious peaks that do not correspond to the velocities in the three-layer model. At negative times, we obtain peaks at multiple times τ that correspond to the interval velocities V_2, V_3, and V_4. It is difficult to make assumptions about the thickness of each layer as in the previous example because of the closely spaced peaks. Notice that in Figure 12a, we do not observe a peak relating to the interval velocity V_4. To record a refraction from the third interface at $r_1 - r_{200}$, we require the source-receiver offset to exceed the critical offset (= 1287 m). Although early source numbers are positioned at far enough distance to fulfill this condition, many sources are not, and a refraction from the third interface is not recorded for these sources. On the other hand, a refraction from the third interface will be recorded and then crosscorrelated at $r_{200} - r_{500}$. This explains why we observe the corresponding peaks in Figure 12b. The above reasoning can also be used to explain why Figure 12b, which considers crosscorrelations between receievers located to the right of the virtual source position, offers better resolution at the correct velocities than Figure 12a, which considers crosscorrelations between receivers located to the left of the virtual source position. The crosscorrelation between reflections will be more prevalent for $r_1 - r_{200}$ and may mask the desired linear refracted energy. The contribution from the crosscorrelation of refractions increases for $r_{200} - r_{500}$ as the source-receiver offset exceeds the critical offset. Figure 12c shows the $\tau - V$ spectrum for $r_1 - r_{250}$ (i.e., to the left of the virtual source) in the virtual source gather of Figure 10b. Figure 12d shows the corresponding $\tau - V$ spectrum for $r_{250} - r_{500}$.

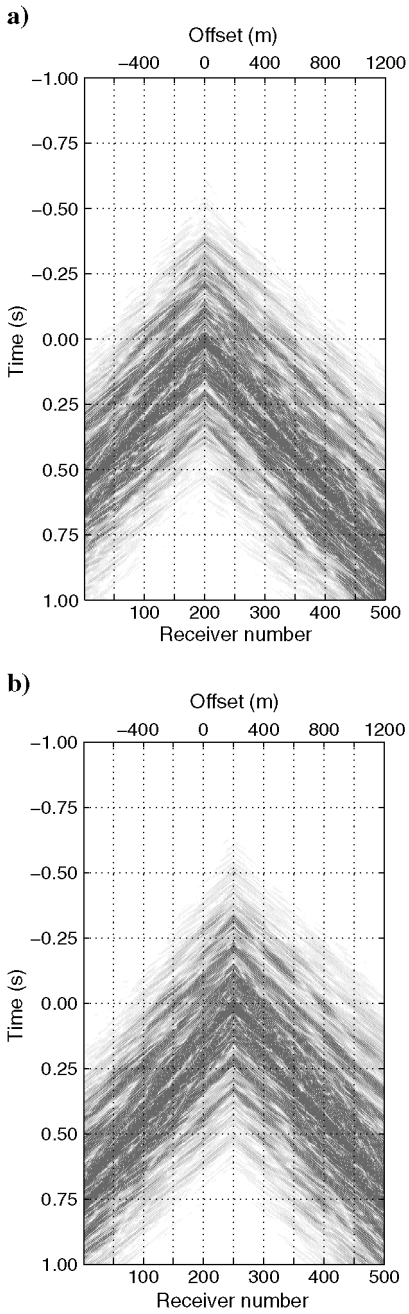

Figure 10. Virtual source gathers for three layer over a half-space model. The virtual source is positioned at (a) r_{200} and (b) r_{250}.

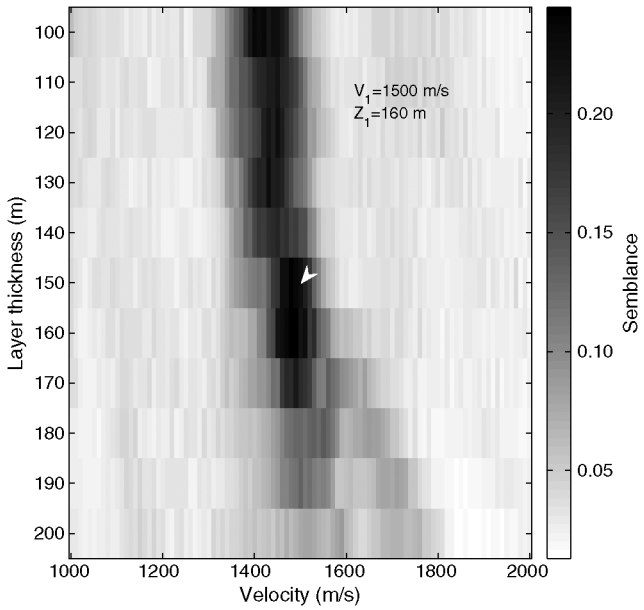

Figure 11. Velocity (V_1) — layer thickness (Z_1) spectrum computed from the correlation gather in Figure 9a using energy up to third-order multiples.

In Figure 12c, we observe peaks at V_2 and V_3. Again for the reasons described above, peaks at V_4 are obtained only in Figure 12d when we consider receivers located to the right of the virtual source position.

We can emphasize the linear nonphysical refractions, and hence, the correct velocities by performing a second crosscorrelation of the virtual source gather. In other words, we produce a new gather by crosscorrelating the Green's function estimate at the virtual source position (i.e., the zero-offset Green's function) with the Green's function estimates at the receivers. The procedure has no physical meaning in seismic interferometry but results in new nonphysical refractions being shifted upward or downward by the arrival times at the virtual source position. Figure 13a shows the $\tau - V$ spectrum obtained after crosscorrelating the estimated Green's functions at $r_{250} - r_{500}$ with the estimated Green's function at r_{250} in the virtual source gather of Figure 10b. At negative times, we achieve two sets of coherent peaks at the correct velocities. Figure 13b shows the velocity panel after stacking the spectrum in Figure 13a at negative times. We achieve three peaks positioned close to the expected velocities. These displays confirm our earlier velocity interpretation in Figure 12.

We now add random noise, bandlimited to match the source signal, to the source gathers before performing interferometry. The signal-to-noise ratio (S/N) is equal to 1. We consider a virtual source positioned at r_{200}. Figure 14a shows the $\tau - V$ spectrum for $r_{200} - r_{500}$. We achieve poorly resolved peaks at V_2 and V_3, but peaks at V_4 are less obvious. We now stack 26 semblance panels that correspond to virtual sources positioned between r_{200} to r_{250} at 2 receiver intervals. Figure 14b shows the resultant $\tau - V$ spectrum. The semblance values are normalized by the number of stacked panels. Much incoherent noise present in Figure 14a is suppressed during stacking. Peaks at V_2 and V_3 are better resolved and we now obtain, although still weak, a set of peaks at V_4.

More realistic 2.5D model

We apply the same methodology to a more realistic model, based on a North Sea oil field (Figure 15a). Figure 15b shows the acquisition geometry. Figure 16 shows the correlation gather for receivers r_1 and r_{35} and Figure 17 shows the corresponding velocity — layer-thickness spectrum computed by using the reflected energy (equation 2) up to the third-order multiples. We obtain the correct velocity and layer thickness of the first layer. Despite the fact that we use a more complex model, our velocity and layer-thickness estimate is better resolved than the corresponding estimates in Figure 6a (single-layer model) and Figure 11 (three-layer model). Compared to those examples, our receivers are positioned closer to the source array and the layer thickness is greater in this example. Hence, there is a well-defined separation between interfering first-layer reflections in the correlation gather, resulting in a better-defined estimate of the subsurface parameters.

Recovery of the first-layer parameters is relatively trivial; however, estimating the deeper velocities is more challenging. We now aim to find the refraction velocities of the deeper layers. Figure 18a, 18b, 18c, and 18d shows the virtual source gathers corresponding to the virtual sources positioned at receivers r_{50}, r_{150}, r_{250}, and r_{350}, respectively. Figure 19a and 19b shows the $\tau - V$ spectra using equation 7 at negative times for $r_1 - r_{50}$ and $r_{50} - r_{450}$ from the virtual source gather in Figure 18a at

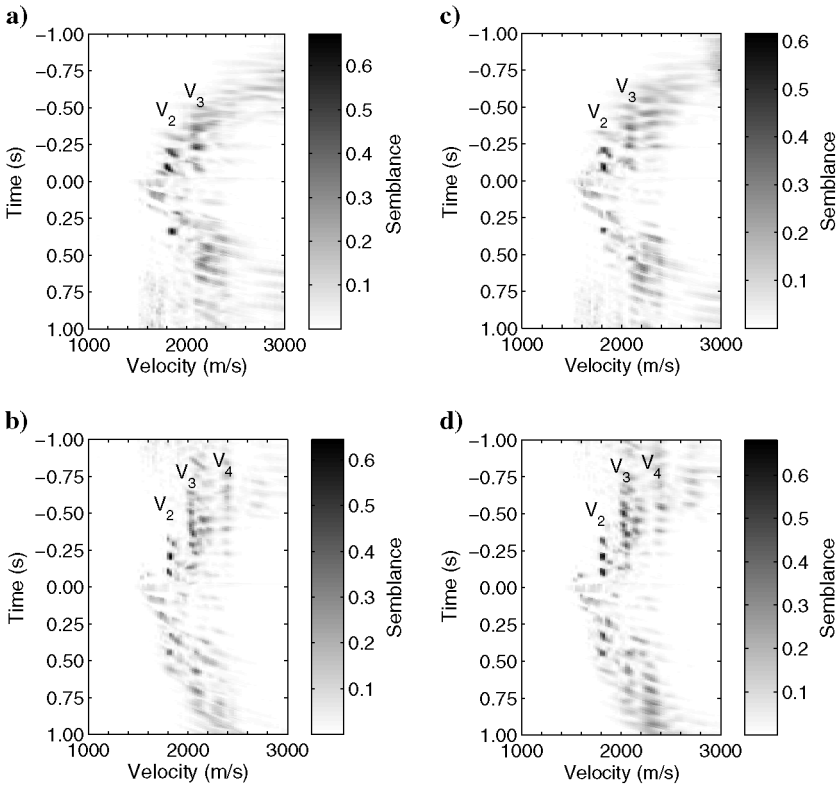

Figure 12. Velocity (V) — time (τ) spectra computed using (a) receivers $r_1 - r_{200}$ and (b) receivers $r_{200} - r_{500}$ of the virtual source gather in Figure 10a, and (c) receivers $r_1 - r_{250}$ and (d) receivers $r_{250} - r_{500}$ of the virtual source gather in Figure 10b.

r_{50}. Figures 19c and 19d show the $\tau - V$ spectra using equation 7 at negative times for $r_1 - r_{150}$ and $r_{150} - r_{450}$ for the virtual source at r_{150}. We include our interpreted velocities. Figure 20 shows the corresponding $\tau - V$ spectra for the virtual source gathers in Figure 18c and 18d. A depth interpretation is difficult from such a display; nevertheless, the velocity spectrum allows us to identify the refraction velocities from a complex model.

DISCUSSION

In general, the S/N of refractions can be highly variable along the receiver array (Palmer, 2001). This factor may impact upon methods that use refractions to determine the seismic velocity. We show that seismic interferometry produces repeating nonphysical refractions whose velocity can be characterized after a $\tau - p$ transform of the virtual source gather. The repeating nature of these spurious arrivals may help identify refraction velocities in noisy field data.

We note that the method presented here has an advantage over conventional velocity analysis. In cases where the seismic velocity is homogeneous in each layer, we can directly estimate the interval velocities from the crosscorrelated refracted energy (as shown in

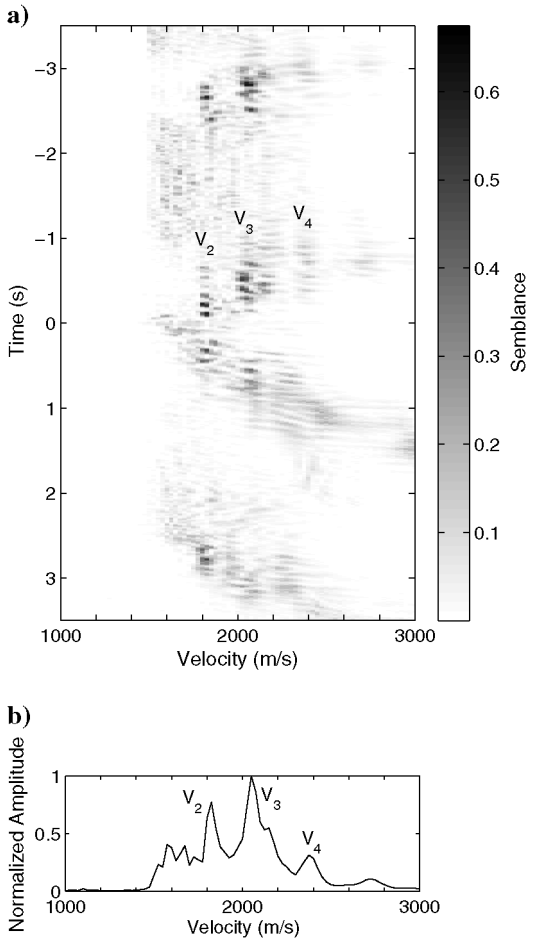

Figure 13. (a) Velocity (V) — time (τ) spectra obtained after crosscorrelating the records at r_{250} with the records at $r_{250} - r_{500}$ in the virtual source gather of Figure 10b. (b) A velocity panel after stacking (a) at negative times.

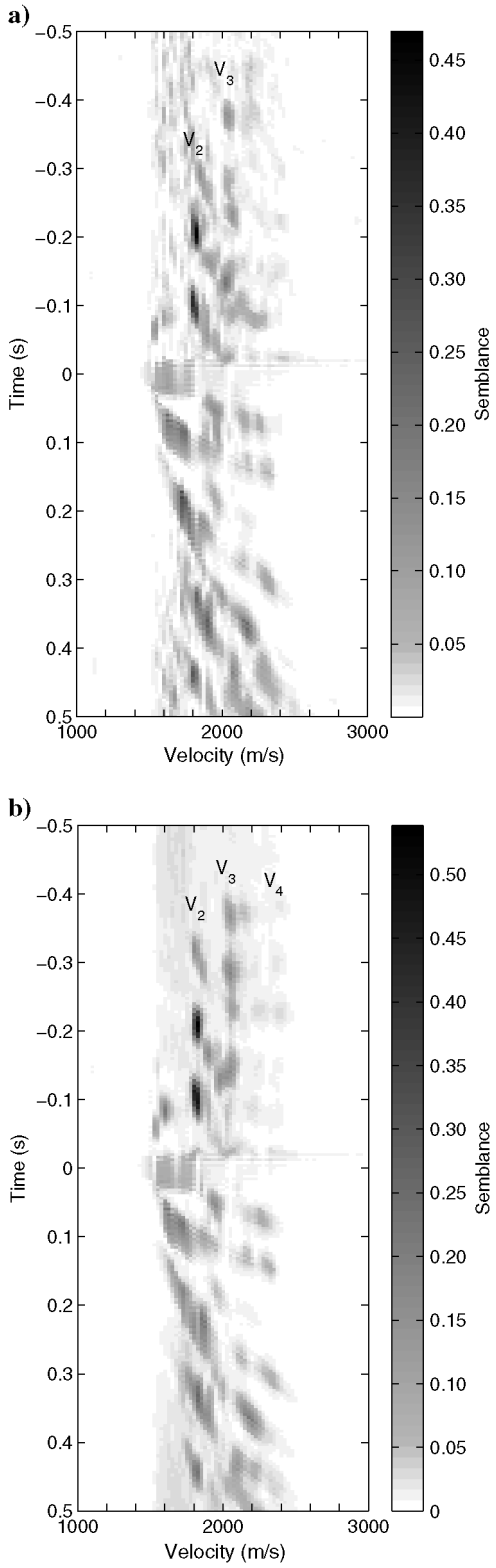

Figure 14. Velocity (V) — time (τ) spectrum computed by using (a) receivers $r_{200} - r_{250}$ of the virtual source gather in Figure 10a, and (b) after stacking 26 semblance panels corresponding to virtual sources positioned at r_{200} to r_{250} at two equal receiver intervals.

Figure 12). Therefore, we eliminate the usual requirement to estimate root mean square velocities as a first step to determine the interval velocity, although we do require long-offset seismic arrays to record the refracted energy.

We have shown that the correlation and virtual source gathers, although linked through seismic interferometry, can be analyzed relatively independently. The correlation gather is dominated by reflected energy, useful for determining the properties of the first

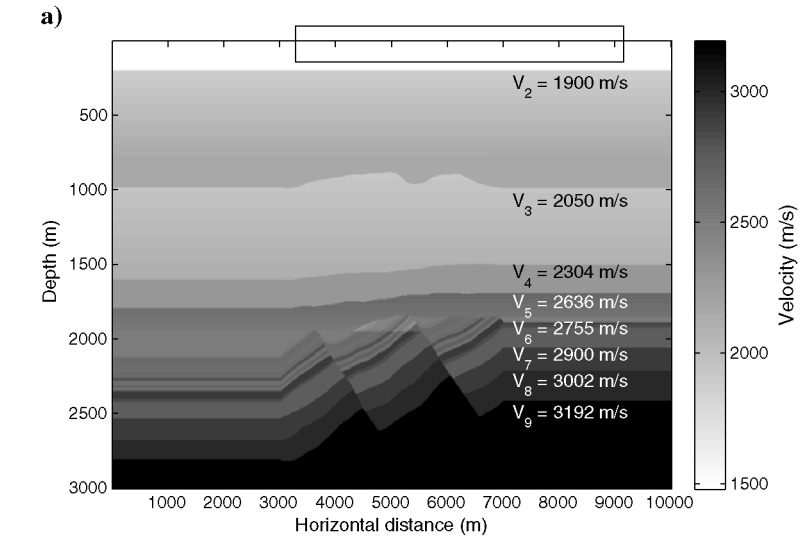

Figure 15. (a) More realistic North Sea model. (b) The acquisition geometry is located within the black box in (a). One hundred (100) sources are now spaced every 25 m and 450 receivers are spaced every 12.5 m.

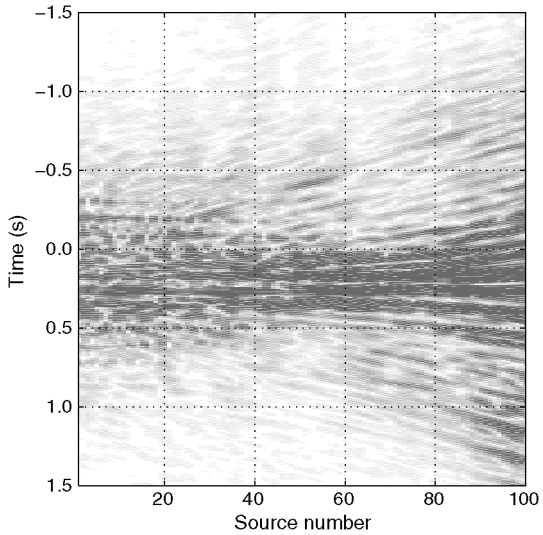

Figure 16. Correlation gather for receiver r_1 and r_{35}, for the North Sea model.

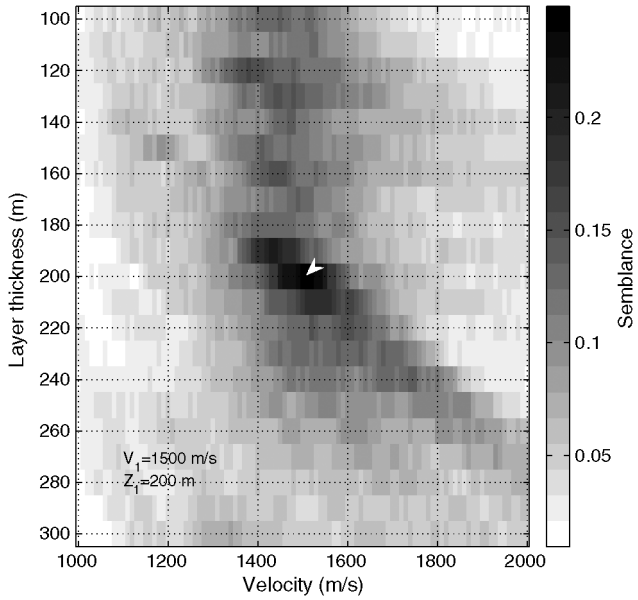

Figure 17. Velocity (V_1) — layer-thickness (Z_1) spectrum computed from the North Sea correlation gather using energy up to the third-order multiples.

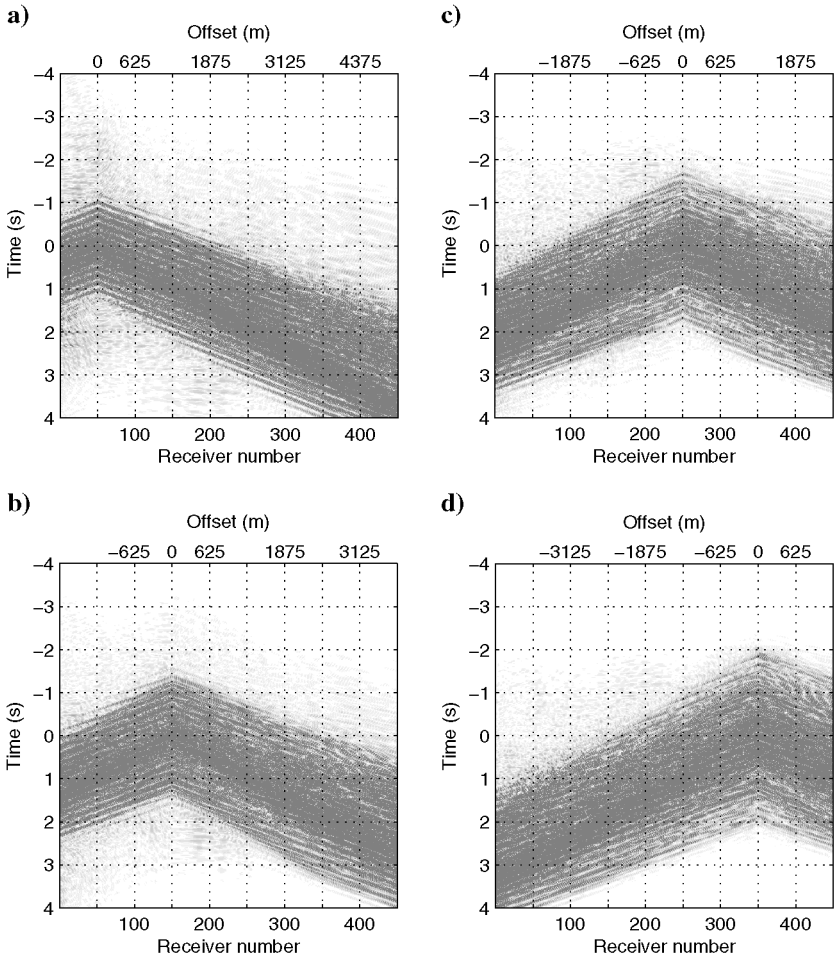

Figure 18. Virtual source gathers for the North Sea model. (a) Virtual source positioned at receiver r_{50}, (b) r_{150}, (c) r_{250}, and (d) r_{350}.

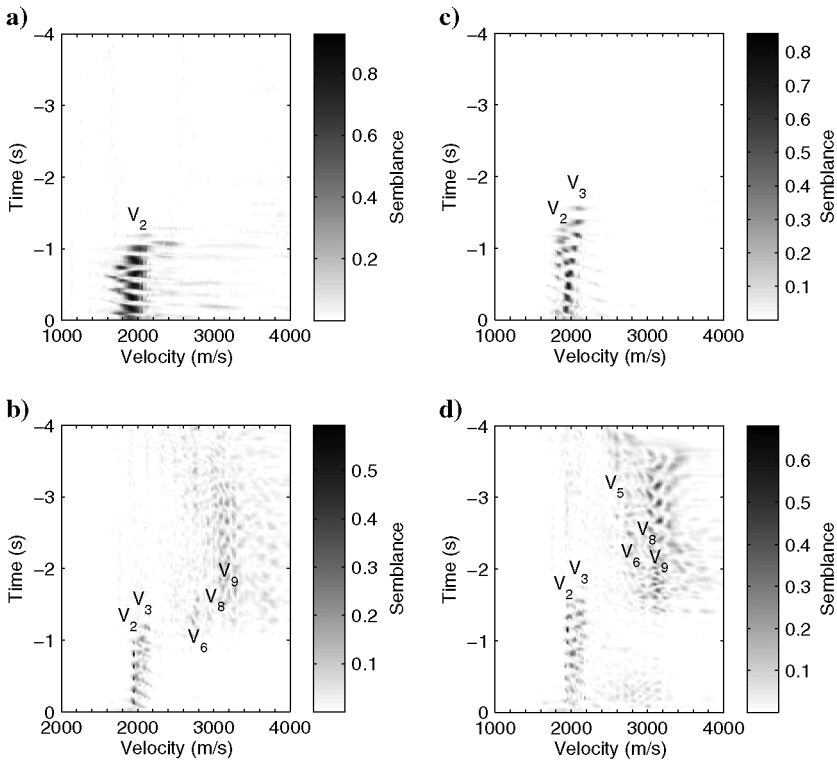

Figure 19. Velocity (V) — time (τ) spectra computed using (a) receivers $r_1 - r_{50}$ and (b) receivers $r_{50} - r_{450}$ from the virtual source at r_{50}, and (c) receivers $r_1 - r_{150}$ and (d) receivers $r_{150} - r_{450}$ from the virtual source at r_{150}.

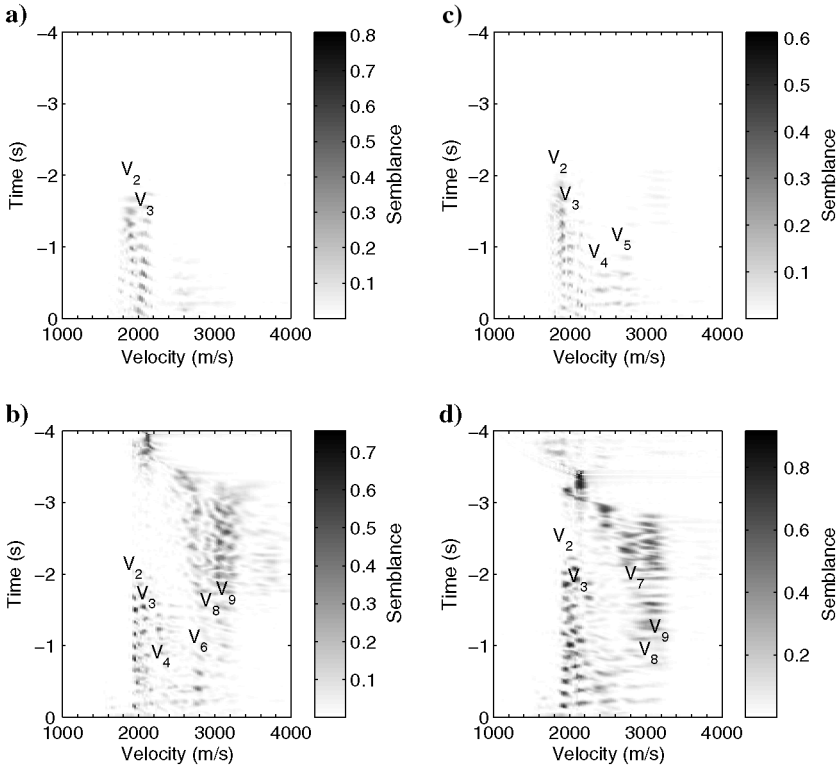

Figure 20. Velocity (V) — time (τ) spectra computed using (a) receivers $r_1 - r_{250}$ and (b) receivers $r_{250} - r_{450}$ from the virtual source at r_{250}, and (c) receivers $r_1 - r_{350}$ and (d) receivers $r_{350} - r_{450}$ from the virtual source at r_{350}.

layer, while the virtual source gather is dominated by nonphysical refracted energy, important for determining the remaining seismic velocities of the deeper layers. Rather than being used as an intermediate step to obtain the virtual source gather, we have shown that the correlation gather contains useful model information in itself.

In this paper, we have shown that if correctly identified, nonphysical energy can be used to extract model information. If we consider a marine-type acquisition geometry, such as that in Figure 1, studies have shown that the stationary-phase points for reflected energy (between one receiver and another receiver at further offset) are positioned at positive times in the correlation gather (Mikesell et al., 2009; King et al., 2011). Therefore, after summation over the source boundary, we expect physical contributions to dominate over nonphysical contributions at positive times in the Green's function estimate. Prior to the stationary-phase point for the primary reflection (e.g., PD in Figure 2b), the crosscorrelation between reflections are nonstationary and sum destructively. We find that the clearest observations of refracted energy are nonphysical and occur prior to the direct arrival away from the aforementioned dominant reflected energy. Nonphysical refractions do exist after the direct arrival (see Figure 5); however, they arrive alongside strong reflected energy and hence, their properties are difficult to extract in a semblance analysis. If we wish to understand the contribution of nonphysical energy in seismic interferometry, we need to analyze the regions in time and space where their contributions impact most. Methods exist to suppress these nonphysical arrivals, or in other words, to enhance the physical arrivals in the Green's function estimates (Mehta et al., 2007; Wapenaar et al., 2008; van der Neut and Bakulin, 2009; Curtis and Halliday, 2010a). We show here that the nonphysical arrivals dominate over the physical arrivals in the case of one-sided illumination. Hence, using the nonphysical arrivals to characterize the model may be more appropriate than suppressing them.

CONCLUSIONS

In seismic interferometry, the Green's functions between two receivers can be extracted by crosscorrelating and summing the Green's functions from an illuminating and surrounding source boundary. The Green's functions obtained in a marine seismic setting with a nonsurrounding source boundary are dominated by nonphysical or so-called spurious arrivals. We show that the imperfect Green's functions still provide important information about the subsurface velocity — essential information for imaging or migration. Unravelling this information can be challenging when nonphysical arrivals dominate the Green's function estimates and bias normal velocity analysis methods. Therefore, new analysis procedures have to be considered.

We show that the reflected and refracted energy in the correlation and virtual source gathers can be analyzed independently and used to obtain information about the seismic velocity of subsurface strata. Specifically, when the source boundary is one-sided and the receivers are positioned at far offset, we show that the crosscorrelations (the Green's functions before summation over the source boundary) are dominated by reflected energy that can be used in a semblance analysis to determine the seismic velocity and thickness of the first layer. Once these crosscorrelations are summed over the boundary of sources, the Green's function estimates are dominated by nonphysical refracted energy. A semblance analysis on these Green's functions determines refraction velocities of the deeper layers. We demonstrate the velocity analysis procedure on a synthetic single layer over half-space model, and a three layer over half-space model before applying the approach to a more realistic

model based on a North Sea oil field. In all examples, we were able to estimate the seismic velocity by using a combination of physical and nonphysical arrivals.

ACKNOWLEDGMENTS

We thank WesternGeco for permission to publish this work. The North Sea synthetic data set was generated as part of collaborative projects between Schlumberger, Lawrence Livermore National Laboratory, and Statoil. We thank Statoil for permission to show the synthetics and Schlumberger for permission to show the results. We acknowledge the support from the Scottish Funding Council for the ECOSSE Joint Research Institute with the Heriot-Watt University, which is a part of the Edinburgh Research Partnership in Engineering and Mathematics (ERPem). We thank Kurang Mehta, Dylan Mikesell, and an anonymous reviewer for suggestions which greatly improved the manuscript.

REFERENCES

Bakulin, A., and R. Calvert, 2006, The virtual source method: Theory and case study: Geophysics, **71**, no. 4, SI139–SI150, doi: 10.1190/1.2216190.

Curtis, A., and D. Halliday, 2010a, Directional balancing for seismic and general wavefield interferometry: Geophysics, **75**, no. 1, SA1–SA14, doi: 10.1190/1.3298736.

Curtis, A., and D. Halliday, 2010b, Source-receiver wave field interferometry: Physical Review E, **81**, 046601, doi: 10.1103/PhysRevE.81.046601.

Curtis, A., H. Nicolson, D. Halliday, J. Trampert, and B. Baptie, 2009, Virtual seismometers in the subsurface of the Earth from seismic interferometry: Nature Geoscience, **2**, 700–704, doi: 10.1038/ngeo615.

Diebold, J. B., and P. L. Stoffa, 1981, The traveltime equation, tau-p mapping, and inversion of common midpoint data: Geophysics, **46**, 238–254, doi: 10.1190/1.1441196.

Forghani, F., and R. Snieder, 2010, Underestimation of body waves and feasibility of surface-wave reconstruction by seismic interferometry: The Leading Edge, **29**, 790–794, doi: 10.1190/1.3462779.

Kennett, B. L. N, 1977, Toward a more detailed seismic picture of the oceanic crust and mantle: Marine Geophysical Researches, **3**, 7–42, doi: 10.1007/BF00309792.

King, S., A. Curtis, and T. L. Poole, 2011, Interferometric velocity analysis using physical and nonphysical energy: Geophysics, **76**, no. 1, SA35–SA49, doi: 10.1190/1.3521291.

Mehta, K., A. Bakulin, J. Sheiman, R. Calvert, and R. Snieder, 2007, Improving the virtual source method by wavefield separation: Geophysics, **72**, no. 4, V79–V86, doi: 10.1190/1.2733020.

Mehta, K., R. Snieder, R. Calvert, and J. Sheiman, 2008, Acquisition geometry requirements for generating virtual-source data: The Leading Edge, **27**, 620–629, doi: 10.1190/1.2919580.

Meissner, R., 1965, Multiple events in refraction shooting: Geophysical Prospecting, **13**, 617–658, doi: 10.1111/gpr.1965.13.issue-4.

Mikesell, D., K. van Wijk, A. Calvert, and M. Haney, 2009, The virtual efraction: Useful spurious energy in seismic interferometry: Geophysics, **74**, no. 3, A13–A17, doi: 10.1190/1.3095659.

Palmer, D., 2001, Imaging refractors with the convolution section: Geophysics, **66**, 1582–1589, doi: 10.1190/1.1487103.

Robertsson, J. O. A., J. O. Blanch, and W. W. Symes, 1994, Viscoelastic finite-difference modeling: Geophysics, **59**, 1444–1456, doi: 10.1190/1.1443701.

Snieder, R., 2004, Extracting the Green's function from the correlation of coda waves: A derivation based on stationary phase: Physical Review E, **69**, 046610, doi: 10.1103/PhysRevE.69.046610.

Snieder, R., K. Wapenaar, and K. Larner, 2006, Spurious multiples in seismic interferometry of primaries: Geophysics, **71**, no. 4, SI111–SI124, doi: 10.1190/1.2211507.

Tatanova, M., A. Bakulin, K. Mehta, V. Korneev, and B. Kashtan, 2008, Reconstructing head waves with virtual source method: 78th Annual International Meeting, SEG, Expanded Abstracts, 183–187.

van der Neut, J., and A. Bakulin, 2009, Estimating and correcting the amplitude radiation pattern of a virtual source: Geophysics, **74**, no. 2, SI27–SI36, doi: 10.1190/1.3073003.

van Manen, D.-J., A. Curtis, and J. O. A. Robertsson, 2006, Interferometric modeling of wave propagation in inhomogeneous elastic media using time reversal and reciprocity: Geophysics, **71**, no. 4, SI47–SI60, doi: 10.1190/1.2213218.

van Manen, D.-J., J. O. A. Robertsson, and A. Curtis, 2005, Modeling of wave propagation in inhomogeneous media: Physical Review Letters, **94**, 164301, doi: 10.1103/PhysRevLett.94.164301.

Wapenaar, K., 2004, Retrieving the elastodynamic Green's function of an arbitrary inhomogeneous medium by cross correlation: Physical Review Letters, **93**, 254301, doi: 10.1103/PhysRevLett.93.254301.

Wapenaar, K., and J. Fokkema, 2006, Green's function representations for seismic interferometry: Geophysics, **71**, no. 4, SI33–SI46, doi: 10.1190/1.2213955.

Wapenaar, K., J. van der Neut, and E. Ruigrok, 2008, Passive seismic interferometry by multidimensional deconvolution: Geophysics, **73**, no. 6, A51–A56, doi: 10.1190/1.2976118.

Yilmaz, Ö., 2001, Seismic data analysis: SEG.